NASA TECHNICAL NOTE

NASA TN D-2022

NASA TN D-2022

AN AEROELASTIC MODEL APPROACH FOR THE PREDICTION OF BUFFET BENDING LOADS ON LAUNCH VEHICLES

by Robert V. Doggett, Jr., and Perry W. Hanson
Langley Research Center
Langley Station, Hampton, Va.

NATIONAL AERONAUTICS AND SPACE ADMINISTRATION • WASHINGTON, D. C. • OCTOBER 1963

TECHNICAL NOTE D-2022

AN AEROELASTIC MODEL APPROACH FOR THE PREDICTION OF BUFFET BENDING LOADS ON LAUNCH VEHICLES

By Robert V. Doggett, Jr., and Perry W. Hanson

Langley Research Center
Langley Station, Hampton, Va.

NATIONAL AERONAUTICS AND SPACE ADMINISTRATION

NATIONAL AERONAUTICS AND SPACE ADMINISTRATION

TECHNICAL NOTE D-2022

AN AEROELASTIC MODEL APPROACH FOR THE PREDICTION OF BUFFET BENDING LOADS ON LAUNCH VEHICLES

By Robert V. Doggett, Jr., and Perry W. Hanson

SUMMARY

A method for determining directly the overall dynamic response in terms of bending moment of an aeroelastic model of a launch vehicle to random (buffet) aerodynamic forces has been applied to two model configurations in the Mach number range from 0.50 to 1.20. The two configurations tested were a blunted cone-cylinder and a bulbous nose with a cylindrical afterbody. The cone-cylinder configuration was free from buffet over the range covered in this investigation. Significant buffet response was measured on the bulbous nose configuration. For this configuration the total buffet response was composed of components associated with the first and second free-free bending modes.

Presented in the appendix is an analysis using the techniques of generalized harmonic analysis which develops in some detail the relationships necessary for predicting full-scale buffet bending moments from data obtained from wind-tunnel tests on dynamically scaled aeroelastic models.

INTRODUCTION

Buffeting of launch vehicles is an important aeroelastic problem area both in terms of the loads experienced by the entire vehicle and of the environment in which a vehicle component may be placed. In several recent launch vehicle failures, buffeting has been suspected as a contributing factor. Since no adequate theoretical method exists for the determination of the magnitudes of the fluctuating loads on a particular configuration, the designer must depend heavily on experimental data. Wind-tunnel buffet studies on aircraft lifting surfaces provided useful information in predicting the buffet characteristics on full-scale components. (See ref. 1, for example.) It is reasonable to assume that similar studies on launch-vehicle models might be equally beneficial. Consequently, an extensive wind-tunnel launch-vehicle buffet study program has been undertaken at the Ames and Langley Research Centers. Most of the data reported to date have been concerned with the fluctuating pressure input part of the problem. For example, in references 2 and 3 measurements have been made of the fluctuating pressures on several different bodies of revolution. In reference 4 fluctuating pressure data are presented for different size models of a large manned launch

vehicle in two different test media. Reference 4 has provided some useful information on the scaling of fluctuating pressure data. Although pressure data play a significant role in understanding the overall buffet characteristics of a particular configuration, application of these input data in the prediction of structural response is usually very difficult. Examples of such an application are given in references 5 and 6.

The present investigation was undertaken to develop a method for determining directly the dynamic response of an aeroelastic launch-vehicle model to random (buffet) aerodynamic forces and to develop relationships useful in predicting full-scale vehicle response from model test results. The method proposed is to conduct wind-tunnel tests on a dynamically scaled aeroelastic model of the launch vehicle. Such a model (acting as a mechanical analog) in a suitable wind tunnel which generates the correct aerodynamic input forces performs the very difficult time and space integrations producing the desired response which can be measured readily.

This method has been applied to an aeroelastic model which was tested over the Mach number range from 0.50 to 1.20. The model response was measured in terms of bending moment by using a resistance-wire strain-gage bridge. The basic configuration tested was a slender blunted cone-cylinder designed to simulate some of the geometric and dynamic characteristics of a representative launch vehicle. The second configuration was a modification of the basic configuration in that the conical nose was replaced with a bulbous nose. The model was supported in such a manner that it was free to respond in simulated free-free bending modes.

Presented in the appendix is an analysis, employing simple beam theory and the techniques of generalized harmonic analysis, which develops relationships useful in scaling model-response data to their corresponding full-scale values.

SYMBOLS

$A(\omega)$ square root of mechanical admittance

$a(t)$ nose amplitude

C generalized damping coefficient

$C(\omega), C_L(\omega), \hat{C}_L(k)$ correlation functions

C_A aerodynamic damping coefficient

C_{cr} critical value of damping

C_c control-system damping

C_h' aerodynamic damping derivative, $2\mu k \frac{C_A}{C_{cr}}$

C_s	structural damping coefficient
$c_L(\xi,t)$	time-dependent section lift coefficient
$\hat{c}_L(t)$	time-dependent effective total lift coefficient
f	natural frequency, $\omega/2\pi$
$h(\xi)$	mode shape based on unit nose deflection
k	reduced frequency, $L\omega/V$
L	total length
l	effective moment arm
M_n	generalized mass
M	Mach number
m	mass per unit length
p_t	stagnation pressure
q	dynamic pressure, $\frac{1}{2}\rho V^2$
R	reference radius
t	time
T	time interval
V	velocity
x	longitudinal coordinate
$y(0,t)$	total nose amplitude
W	total weight
α	angle of attack
θ	phase angle
σ^2	mean-square bending moment
σ	root-mean-square bending moment
σ_T	total root-mean-square bending moment

σ_t total root-mean-square bending moment associated with response in first two free-free bending modes, $\sqrt{\sigma_1^2 + \sigma_2^2}$

ξ nondimensional longitudinal coordinate, x/L

ξ_o any particular nondimensional longitudinal station

$\Phi_y(0,\omega)$ power spectral density of nose deflection

ω circular frequency, $2\pi f$

ρ air density

μ mass ratio, $M/\rho\pi R^2 L$

Λ product of lengths, $L^2R^2l_n^2$

Subscripts:

F full scale

M model

m mth natural free-free bending mode, m = 1, 2, 3, . . .

n nth natural free-free bending mode, n = 1, 2, 3, . . .

Dots over symbols indicate derivative with respect to time.

APPARATUS AND TECHNIQUE

Wind Tunnel

The Langley 8-foot transonic pressure tunnel was used in this investigation. This facility is a slotted-throat single-return wind tunnel capable of continuous operation throughout the transonic speed range at stagnation pressures from 1/4 to 2 atmospheres. Both test-section Mach number and density are continuously controllable.

Model

In order to examine the aeroelastic model approach in predicting full-scale buffet loads, a simple aeroelastic model was designed. The geometric and dynamic properties of the model were chosen to be representative of those scaled from a typical launch vehicle; however, for simplicity, the model was designed to be approximately a uniform beam as far as its mass and stiffness distributions are concerned.

Two different configurations were studied in this investigation and their geometries are shown in figure 1. Configuration 1 was a blunted cone-cylinder, having a 14.5° semivertex angle conical nose mounted on a cylindrical afterbody with a fineness ratio of 8.99. Configuration 2 was a modification of configuration 1. The conical nose was replaced with a 29° semivertex angle conical bulbous nose (has a reflex angle downstream of the maximum diameter). The afterbody fineness ratio for this configuration was 7.66. The ratio of maximum nose diameter to afterbody diameter was 1.6.

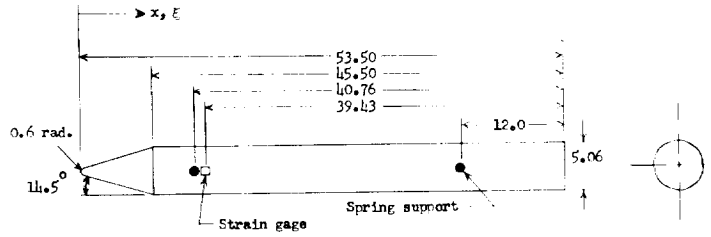

(a) Configuration 1.

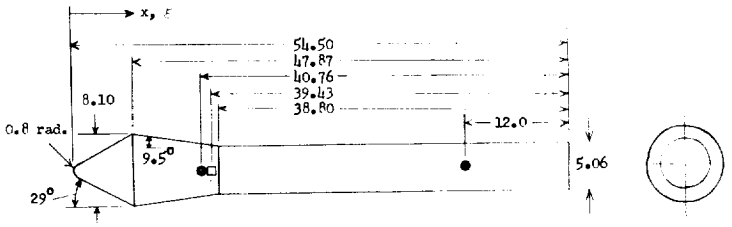

(b) Configuration 2.

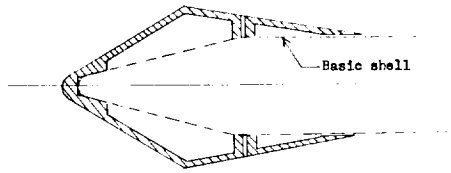

(c) Longitudinal section through nose of configuration 2.

Figure 1.- Line drawings of configurations tested. All dimensions are in inches unless otherwise noted.

Some of the details of model construction and mounting system are illustrated in figure 2. The shaker shown mounted on the sting in figure 2 was used for aerodynamic damping measurements presented in reference 7. The model "snubber" was used to restrain the model response when data were not being taken. To facilitate assembly, the model was made in three sections. The model consisted of a 0.03-inch-thick fiber-glass cylindrical shell which was radially stabilized by several aluminum-alloy rings spaced at intervals of approximately 5 inches over the length of the model. The longitudinal bending stiffness of the model was governed by the stiffness of the fiber-glass shell. Scaled model natural bending frequencies approximating those of a typical large launch vehicle were obtained by attaching lead ballast weights to the aluminum-alloy rings. The bulbous nose, which was made of wood and fiber glass, was slipped over the conical nose of configuration 1 to form configuration 2. (See fig. 1(b).) Some of the ballast weight was removed to compensate to some degree for the weight of the bulbous nose section.

The model was sting mounted. It was attached to the sting by two pairs of soft flex springs. A photograph of a typical set of springs is shown in figure 2(b). The springs were attached to the model near the nodal points of the first free-free bending mode in order to minimize the influence of the springs on the free-free modes. An effort was made to determine the effect of the springs

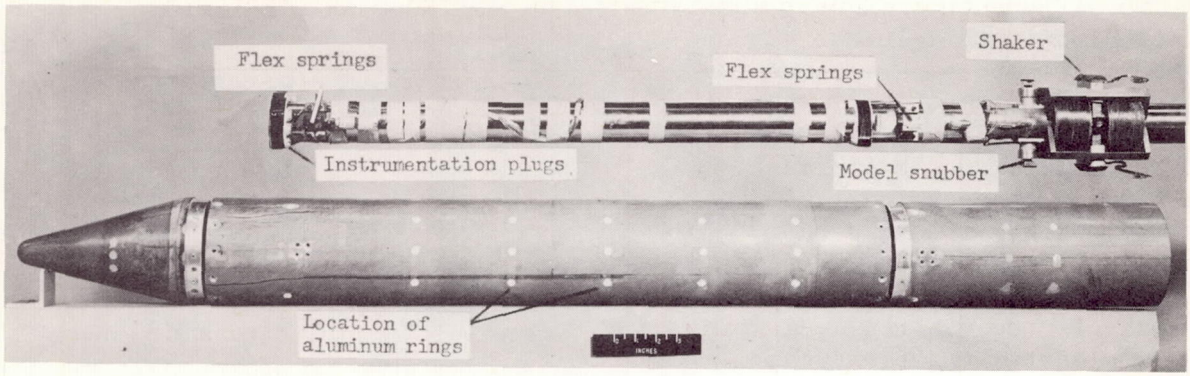

(a) General view of model configuration 1 and sting support.

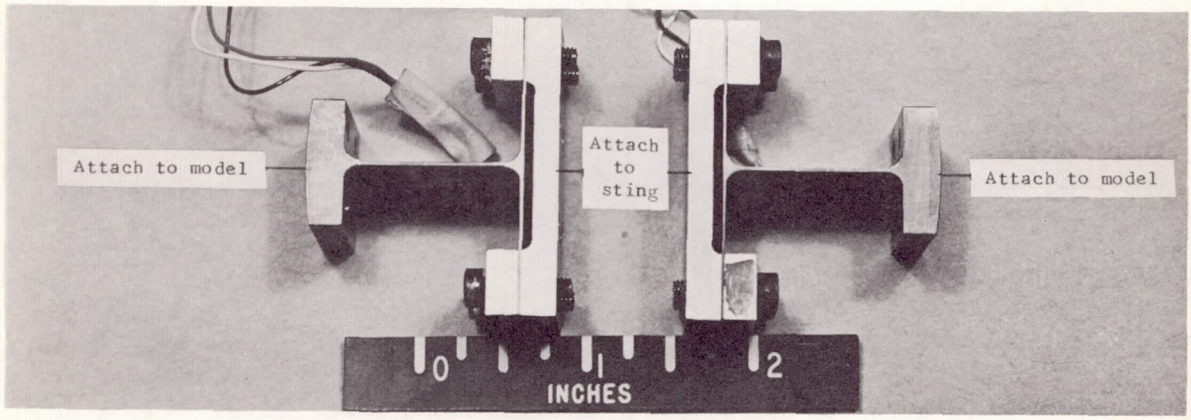

(b) General view of a pair of model support springs. L-63-4738

Figure 2.- Photographs of model and sting assembly, and support springs.

on the frequencies of the first three modes of configuration 1 by supporting the model at the node lines on soft rubber supports. The natural frequencies and corresponding node lines obtained from these tests when compared with those measured with the model mounted on the sting indicated that the effect of the attachment springs was negligible.

The physical properties of the two configurations are presented in tables I and II and in figure 3. The model natural frequencies are presented in table I along with the corresponding structural damping ratios. The structural damping was somewhat amplitude- and temperature-dependent. (See ref. 7.) The values presented in the table are average values. The mass properties are presented in table II. The mass distribution was obtained by weighing the model components prior to assembly. The generalized masses were calculated from the experimental mode shapes and mass distributions. Presented in figure 3 are the measured normalized mode shapes for the first two free-free bending modes for both configurations. No mode shapes are presented for the third free-free bending modes since these modes contained relatively large deflections in the "hoop" plane (involving

TABLE I.- MODEL FREQUENCY AND DAMPING CHARACTERISTICS

Configuration 1		Configuration 2		Remarks
f	C_s/C_{cr}	f	C_s/C_{cr}	
11	(a)	12	(a)	Sting mode
22	(a)	23	(a)	Rigid body pitching mode
32	(a)	37	(a)	Rigid body translation mode
85	0.0085	79	0.011	First free-free bending mode
223	0.013	206	0.010	Second free-free bending mode
387	(a)	333	(a)	Third free-free bending mode

[a]Not obtained.

deformations of the cross section). The mode shapes were determined by exciting the model at resonance at constant amplitude and measuring the response with a small velocity pickup. Also included in figure 3 are the first two natural free-free bending mode shapes and frequencies for a uniform beam having the same total mass and effective stiffness as the model configurations. As is shown on the figure, the mode shapes for the model tested in this investigation are very similar to those of a uniform free-free beam.

Instrumentation and Calibration

The instrumentation used in this investigation are shown schematically in figure 4. The dynamic bending moments were indicated by a suitably calibrated four-active-arm resistance-wire strain-gage bridge bonded to the model fiber-glass shell. The location of the electrical center of the bridge is shown in figure 1. The bridge output signal was amplified by a 3-kilocycle carrier amplifier. The amplified signal was recorded on a 6.75-kilocycle frequency-modulated tape recorder and monitored on a true-root-mean-square vacuum tube voltmeter. An alternating-current calibration signal was also recorded periodically by using a variable-frequency audio oscillator. The relationship between strain-gage bridge output signal and applied bending moment was obtained from a static calibration. To verify that the strain-gage bridge was sensitive to bending strains only, two calibration procedures were used. With the model mounted as a simply supported beam, known shear loads were applied and produced known bending moments about the strain-gage bridge electrical center due to support reaction forces. The bridge output, or unbalance, was read by using a self-balancing potentiometer.

TABLE II.- MASS DISTRIBUTION

Configuration 1: W = 19.68 lb; M_1 = 0.1081 slug; M_2 = 0.0740 slug	
ξ	m, slugs/ft
0	
.0136	0.0155
.0271	.0155
.0550	.0155
.0818	.0155
.0958	.4385
.1355	.0155
.1542	.1650
.1682	.8975
.1720	.0155
.2172	.0155
.2312	.7485
.2579	.0155
.2748	.0155
.3302	.0155
.3442	.8375
.4121	.0155
.4291	.8695
.5000	.0155
.5140	.8735
.5845	.0155
.5985	.8725
.6700	.0155
.6870	.8125
.7475	.0155
.7620	.1247
.7800	.6260
.8460	.0155
.8550	.0607
.8870	.0155
.9000	1.1275
.9460	.0155
.9600	.2257
1.0000	.0155

Configuration 2: W = 21.29 lb; M_1 = 0.1150 slug; M_2 = 0.0562 slug	
ξ	m, slugs/ft
0	
.0180	0.0180
.0313	.0414
.0446	.0598
.0720	.0348
.0983	.0428
.1120	.4700
.1511	.0504
.1695	.2000
.1832	1.0362
.1896	.1424
.2313	.0453
.2451	.7761
.2713	.0416
.2880	.0296
.3423	.0155
.3560	.8375
.4230	.0155
.4396	.8695
.5090	.0155
.5230	.8735
.5925	.0155
.6060	.8725
.6765	.0155
.6930	.8125
.7520	.0155
.7665	.1247
.7840	.6260
.8490	.0155
.8580	.0607
.8890	.0155
.9020	1.1275
.9470	.0155
.9610	.2257
1.0000	.0155

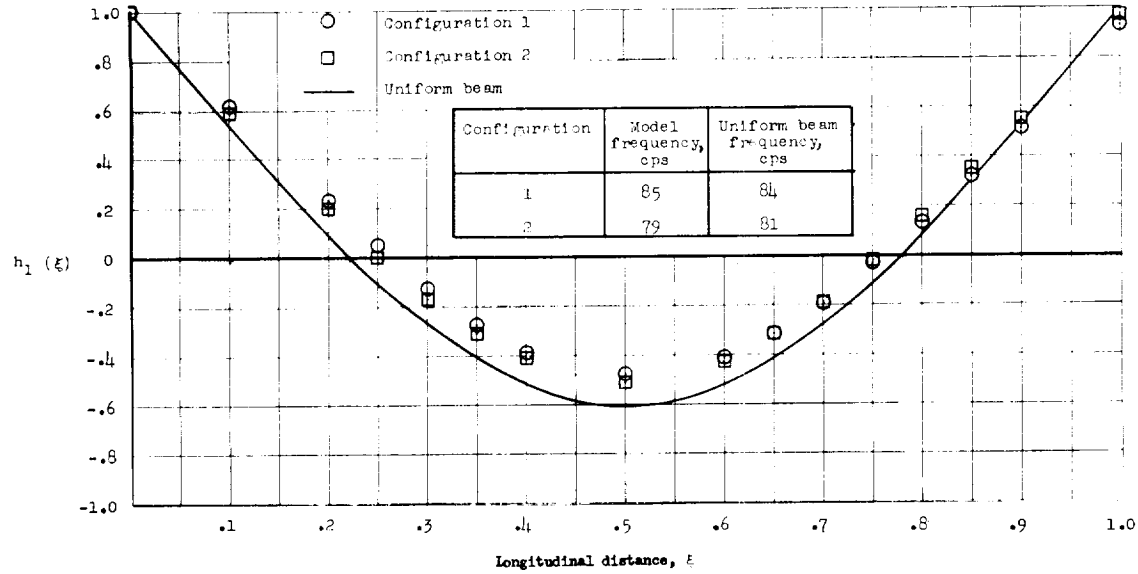

Configuration	Model frequency, cps	Uniform beam frequency, cps
1	85	84
2	79	81

(a) First free-free mode.

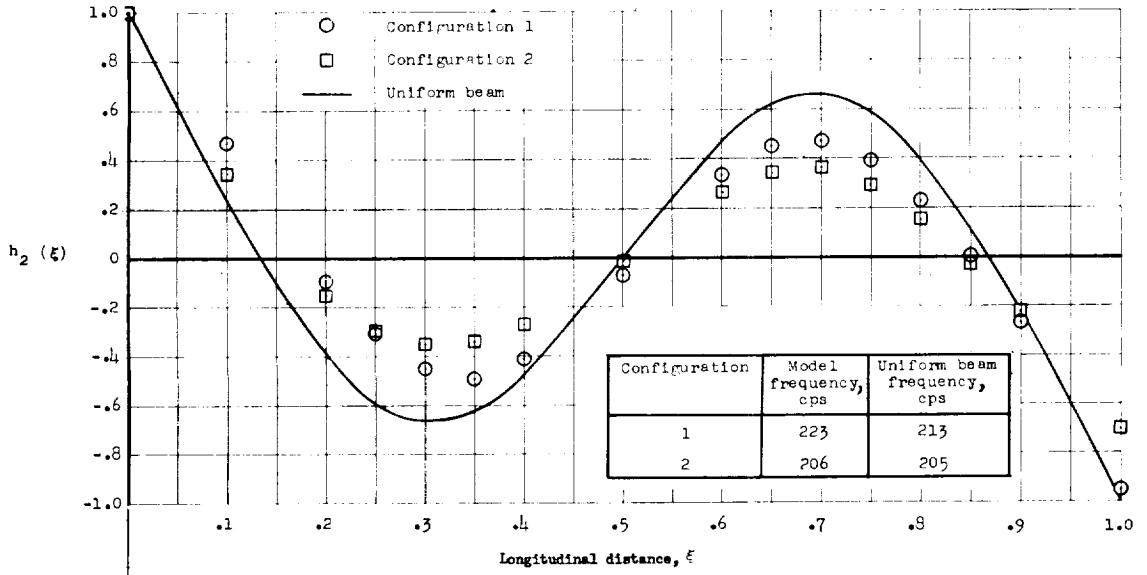

Configuration	Model frequency, cps	Uniform beam frequency, cps
1	223	213
2	206	205

(b) Second free-free mode.

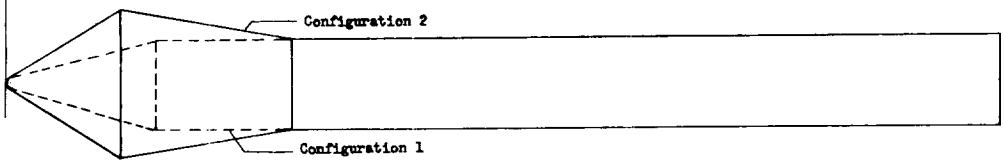

(c) Configurations.

Figure 3.- Measured mode shapes for first and second free-free bending modes.

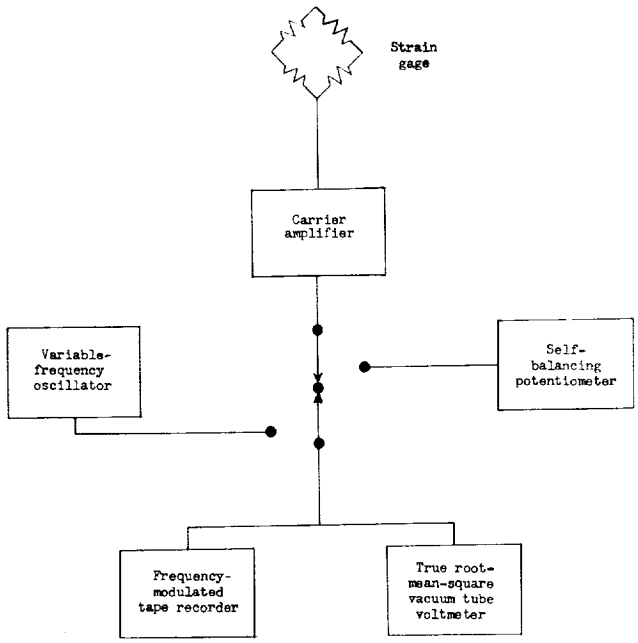

Figure 4.- Schematic diagram of data-recording instrumentation.

A similar calibration was made where known couples were applied about the strain-gage bridge location. The results of this calibration were in good agreement with the one where the moments were produced by shear loads. Therefore, it was concluded that the strain-gage bridge was sensitive to bending strains only.

Test Conditions and Procedure

Dynamic bending-moment measurements were made on configuration 1 at angles of attack of 0° and 4° throughout the Mach number range from 0.50 to 1.20 at a stagnation pressure of 1,800 pounds per square foot. Similar measurements at an angle of attack of 0° were made on configuration 2 at a stagnation pressure of 600 pounds per square foot over the Mach number range from 0.50 to 1.15. One data point for configuration 2 was taken at a Mach number of 0.90 and a stagnation pressure of 1,800 pounds per square foot. Configuration 2 was not tested throughout the Mach number range at a stagnation pressure of 1,800 pounds per square foot since at this pressure the model response was so large that failure of the support springs resulted after only 1 or 2 minutes of exposure (snubbers retracted). The tunnel stagnation temperature was held constant at 120° F for all test conditions. The variation of the test dynamic pressure and Reynolds number for both configurations is shown in figure 5. The Reynolds number was based on the model diameter at the base of the conical nose section for both configurations. These lengths were 5.06 and 8.10 inches for configurations 1 and 2, respectively.

The procedure for a typical test point was as follows: The test-section Mach number and density were adjusted until the desired flow conditions were obtained. The model "snubber" was then retracted, and the model was allowed to respond to the aerodynamic forces present. A 45-second sample of the strain-gage output signal was recorded on the tape recorder. The root-mean-square value of the strain-gage bridge signal was read by using the true-root-mean-square vacuum-tube voltmeter. The model "snubber" was actuated and this procedure repeated until sufficient data had been determined to cover the Mach number range of interest.

Data Reduction

Some of the data recorded on the magnetic tape were reduced to power spectral densities by the use of an electronic analog analyzer. The tape-recorded data were analyzed in the frequency range from 0 to 500 cycles per second by using a

6.79-cycle-per-second bandpass filter. Overall root-mean-square values of the tape-recorded signals were obtained by an electronic analysis. Root-mean-square values obtained by using the electronic analysis were in good agreement with the root-mean-square values obtained by using the true-root-mean-square vacuum-tube voltmeter while the tests were being conducted. The electrical signals were converted to bending moment by using the strain-gage calibration constant.

For configuration 2 the bending moment associated with response in each of the first two free-free bending modes was obtained by integrating the power spectra in the neighborhood of the resonant frequency of the desired mode. For the first mode the range of integration was from about 50 cycles per second to 125 cycles per second and was from about 160 cycles per second to 240 cycles per second for the second mode. Modal bending moments were not determined for configuration 1 because of the relatively low level response obtained for this model.

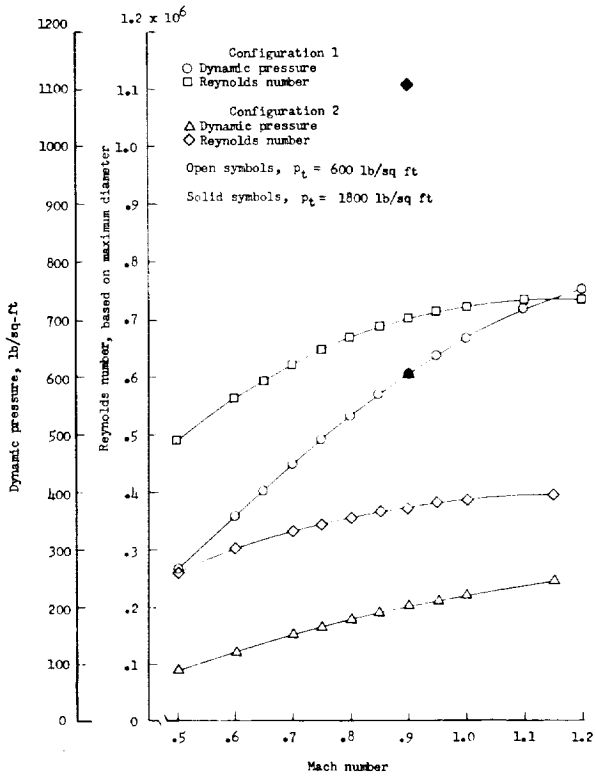

Figure 5.- Variation of test dynamic pressure and Reynolds number with Mach number.

ANALYSIS

For wind-tunnel buffet studies on launch-vehicle models to be useful in predicting full-scale buffet loads, the necessary model—full-scale scaling relationships must be known. A dynamic analysis of launch-vehicle buffeting has been considered in some detail in the appendix. In the analysis, based on the techniques of generalized harmonic analysis, the vehicle was assumed to be flying at constant altitude with a constant velocity. The only aerodynamic forces present in addition to the random component were damping forces proportional to the velocity of the bending vibrations of the system. No loss of generality results from neglecting the aerodynamic inertia and spring forces since such forces usually are small when compared with their structural counterparts for a slender launch vehicle. (See, for instance, refs. 7 and 8.) Structurally, the vehicle was considered to be a linear multi-degree-of-freedom system.

The final result obtained from this analysis for the total root-mean-square bending moment at some longitudinal station ξ_o is

$$\sigma_T^2(\xi_0) = \sum_{n=1}^{\infty} l_n^2 \left[\frac{\pi\omega_n}{4\left(\frac{C}{C_{cr}}\right)_n}\right] q^2 R^2 L^2 \frac{L}{V} \hat{C}_{L,n}(k_n) \tag{1}$$

The total mean-square bending moment is a superposition of single-degree-of-freedom results, coupling terms having been neglected in the development and each mode being independently treated as a separate system. (See appendix.) The general term of the series in equation (1) is essentially the same solution that would be obtained for a single-degree-of-freedom system subjected to a random loading. (See ref. 1.) The right-hand side of equation (1) may be conveniently separated into three parts. The first part, the term l_n^2 is the square of an effective moment arm. The second term, enclosed in brackets, is an admittance-type term. In particular, it is $\pi/2$ times the maximum value of the mechanical admittance in the nth mode multiplied by the width of the admittance curve at the one-half-power point. The damping ratio which appears in the second term of the right-hand side of equation (1) is

$$\left(\frac{C}{C_{cr}}\right)_n = \left(\frac{C_c}{C_{cr}}\right)_n + \left(\frac{C_s}{C_{cr}}\right)_n + \left(\frac{C_A}{C_{cr}}\right)_n$$

where

$\frac{C_A}{C_{cr}}$ aerodynamic damping ratio

$\frac{C_c}{C_{cr}}$ control-system damping ratio

$\frac{C_s}{C_{cr}}$ structural damping ratio

In the notation of reference 7 the aerodynamic damping ratio is related to the effective aerodynamic damping derivative $C_h^{\bullet}$ by

$$\frac{C_A}{C_{cr}} = \frac{C_h^{\bullet}}{2\mu k}$$

The remaining terms are associated with the random aerodynamic loading. The function $\hat{C}_{L,n}(k_n)$ is the correlation function of the random section lift coefficients for the nth mode. Although not mathematically exact, a convenient way of thinking of this function is that it is the power spectrum of an effective random aerodynamic coefficient in the nth mode.

The use of equation (1) for scaling buffet loads is readily apparent. Since the reduced frequency $k_n = \frac{L\omega_n}{V}$ and $\hat{C}_{L,n}(k_n)$ would be the same for both a dynamically scaled aeroelastic model and the full-scale vehicle, the full-scale bending moment for the nth mode is related to the corresponding model value by

$$\sigma^2(\xi_o)_{n,F} = \left(\frac{L_F}{L_M}\right)^6 \frac{\left[\left(\frac{C_s}{C_{cr}}\right)_n + 2\pi R^2\left(\frac{C_{\dot{h}}}{C_{cr}}\right)_n \frac{q}{V}\right]_M}{\left[\left(\frac{C_s}{C_{cr}}\right)_n + \left(\frac{C_c}{C_{cr}}\right)_n + 2\pi R^2\left(\frac{C_{\dot{h}}}{C_{cr}}\right)_n \frac{q}{V}\right]_F} \frac{q_F^2}{q_M^2} \sigma^2(\xi_o)_{n,M} \qquad (2)$$

The total mean-square bending-moment relationship between full-scale vehicle and model is

$$\sigma^2(\xi_o)_{T,F} = \sum_{n=1}^{\infty}\left(\frac{L_F}{L_M}\right)^6 \frac{\left[\left(\frac{C_s}{C_{cr}}\right)_n + 2\pi R^2\left(\frac{C_{\dot{h}}}{C_{cr}}\right)_n \frac{q}{V}\right]_M}{\left[\left(\frac{C_s}{C_{cr}}\right)_n + \left(\frac{C_c}{C_{cr}}\right)_n + 2\pi R^2\left(\frac{C_{\dot{h}}}{C_{cr}}\right)_n \frac{q}{V}\right]_F} \frac{q_F^2}{q_M^2} \sigma^2(\xi_o)_{n,M} \qquad (3)$$

Although the full-scale bending moment at a particular location along the vehicle can be determined directly from equation (3), the missile or launch-vehicle designer needs to know the distribution of bending moments along the structure. Therefore, in making dynamic bending-moment measurements on a model using a single strain-gage bridge, a strain-gage location sensitivity factor must be determined since a bridge located say at the point of maximum bending moment in the first mode may not be very sensitive to moments produced by response in the second mode. The necessary sensitivity factors were determined for the first two modes of both model configurations by calculating the bending-moment distribution due to inertia loading for motion in each mode. These distributions were calculated by using the experimentally determined mode shapes and mass distributions and are presented in figure 6 for configuration 2 in terms of percent maximum bending moment. The corresponding distributions for configuration 1 were very similar to those of configuration 2. The strain-gage bridge location sensitivity factors measured in terms of the ratio of bending moment about the strain-gage location to maximum moment in a particular mode are presented in table III. As is indicated by the data in the table, the strain-gage sensitivities were approximately the same for both model configurations.

RESULTS AND DISCUSSION

A method for determining directly the dynamic response of an aeroelastic launch-vehicle model to random (buffet) aerodynamic forces has been applied to two model configurations. The basic concept of this method is the direct measurement of bending moments induced on an aeroelastic model supported in such a

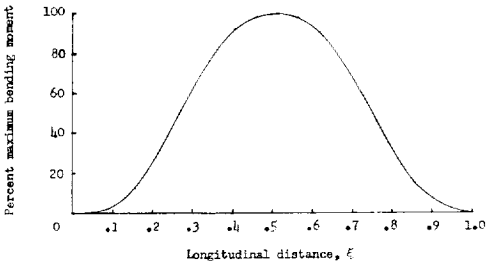

(a) First free-free mode.

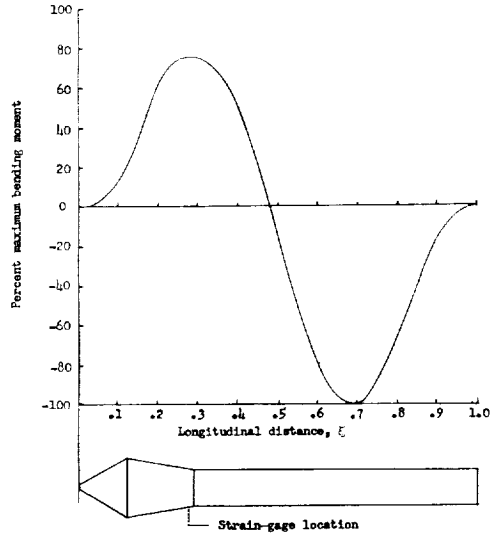

(b) Second free-free mode.

Figure 6.- Calculated bending-moment distribution for the first and second free-free bending modes of configuration 2.

TABLE III.- STRAIN-GAGE LOCATION SENSITIVITY FACTORS

Configuration	Free-free bending mode	Strain-gage location sensitivity factor
1	1	0.436
	2	0.794
2	1	0.521
	2	0.752

manner that it is free to respond in its free-free bending modes. The results of this investigation are presented in figures 7 to 11.

The bending moments measured on the two configurations are compared in figure 7 as a function of Mach number. Since tests were conducted at different levels of dynamic pressure, it was necessary to determine a parameter which would remove the effects of different flow conditions from the model data. A dynamic analysis of buffeting based on the techniques of generalized harmonic analysis (see appendix) indicates that for a system with only structural damping, the root-mean-square bending moment is directly proportional to dynamic pressure for a given Mach number. The results of reference 7 indicate that the aerodynamic damping for the two configurations studied in this investigation is small when compared with the structural damping for the range of flow conditions covered. Therefore, the aerodynamic damping was neglected and the bending-moment data are presented in the form of the ratio of root-mean-square bending moment to dynamic pressure. (It is of interest to note that in aircraft wing and/or tail buffet studies it is the structural damping that is usually assumed to be small. (See ref. 1.) For this case when the structural damping is negligible, the dynamic analysis of buffeting indicates that the root-mean-square buffet bending moments would vary linearly with the square root of dynamic pressure.) Data taken at angles of attack of 0° and 4° are presented in figure 7 for configuration 1. The data for configuration 2 were taken at an angle of attack of 0°. As is indicated by the data in figure 7 there is quite a difference in level of bending moment when comparing the results for the two configurations. The bending moments obtained for configuration 1 are believed to be produced by the response of the model to residual wind-tunnel turbulence. This belief is substantiated by the agreement of the data for the two different angles of attack,

since it would be expected that buffet bending moments would vary with angle of attack. The response of the bulbous nose model is attributed to buffeting. It should be pointed out that the aerodynamic damping for configuration 1, although small when compared with the structural damping, was positive (stable) over the test range covered. The aerodynamic damping for configuration 2, also small, does become negative (unstable) over a small Mach number range near 0.95. (See ref. 7.) The total damping, including both aerodynamic and structural components, was positive. An estimate of the total bending moment for configuration 2 which is actually due to buffeting can be made by using the data for the cone-cylinder model as a tare value since both models have similar dynamic characteristics and approximately equal strain-gage location sensitivities. That is, that part of the total response for configuration 2 which is due to wind-tunnel turbulence would be approximately equal to the total bending-moment response measured for configuration 1.

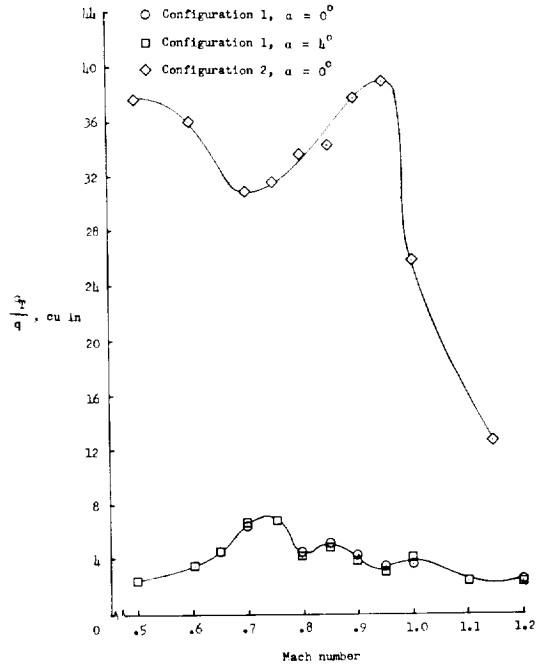

Figure 7.- Variation of ratio of total root-mean-square bending moment at strain-gage location to dynamic pressure with Mach number for configurations 1 and 2.

As pointed out in the section entitled "Analysis," it is necessary to determine the distribution of energy throughout the frequency spectrum in addition to determining the overall energy level if the model data are to be scaled to full-scale values. Presented in figure 8 are sample bending-moment power spectral densities for both of the model configurations investigated. These spectra are from data taken at a Mach number of 0.90, and a dynamic pressure of 603 pounds per square foot. As is seen from figure 8 there are peaks in the spectra associated with the natural frequencies of the two configurations. The maximum values of the peaks obtained for configuration 2 are considerably higher than those obtained for configuration 1. Most of the power is contained in the peaks associated with the free-free bending modes. In the frequency range from 0 to about 40 cycles per second, there is a small amount of power. There are three resonant frequencies in this range, a sting bending mode, model rigid-body pitching mode, and model rigid-body translation mode. The sting and rigid-body translation modes are extraneous in that they would not be present for an actual launch vehicle in flight. A nonzero rigid-body pitch frequency would appear since aerodynamic and engine stiffnesses are present. Similar extraneous modes would appear for any wind-tunnel model. Since these extraneous modes do not have resonances near those of the free-free bending modes, and soft springs were used to support the model on the sting, the support spring effectively isolated the model response from sting motions. This result is illustrated in figure 9 which shows the variation with Mach number of the ratio of root-mean-square bending moment attributable to response in the first two free-free bending modes for configuration 2 to total root-mean-square

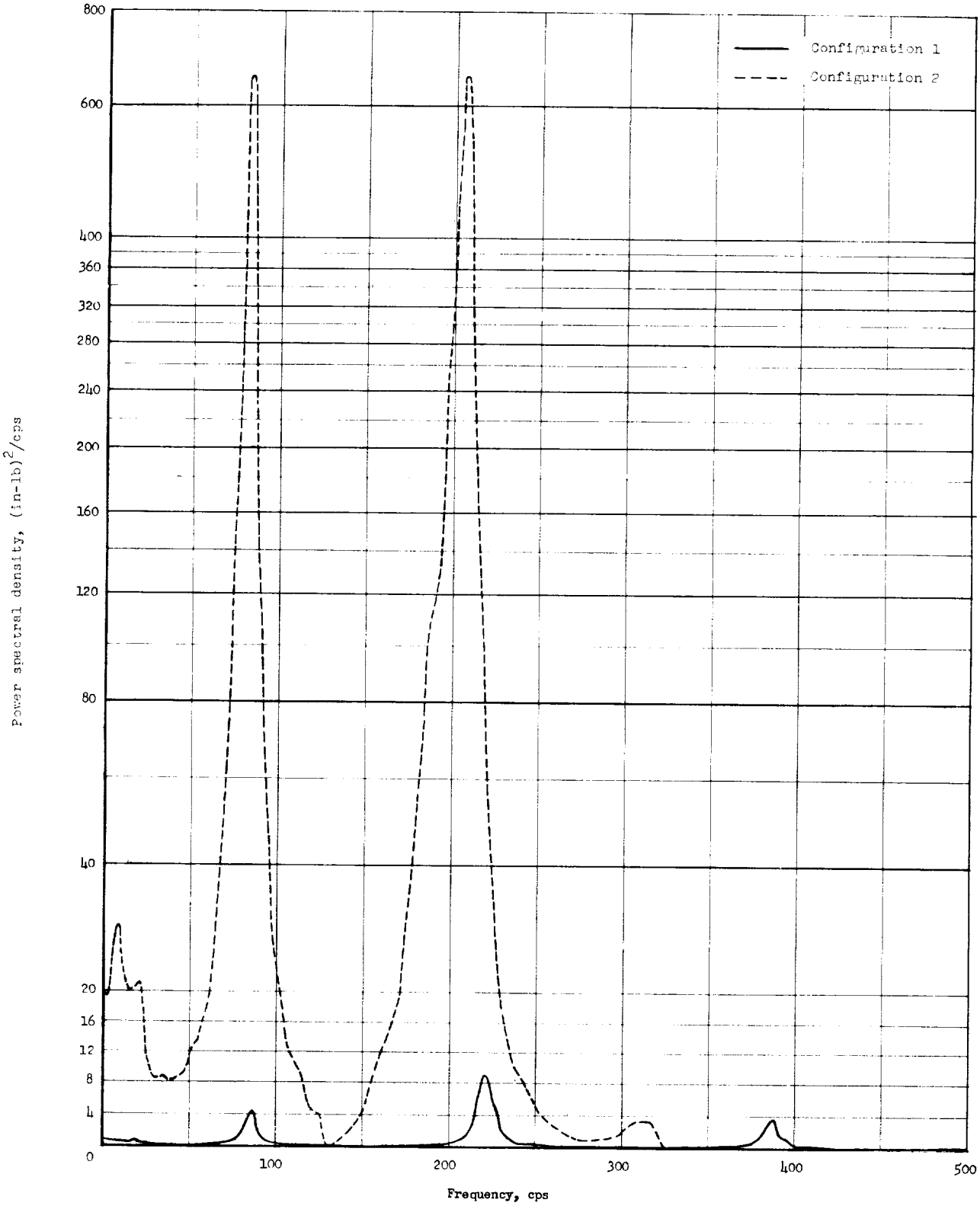

Figure 8.- Sample power spectra. M = 0.90 and q = 603 pounds per square foot.

bending moment. The deviation of this ratio from unity is a measure of the energy contained in all modes excluding the first two bending modes. As is seen from figure 9, these deviations are relatively small for all Mach numbers except for $M = 0.50$. Since examination of the power spectral densities indicated that most of the response other than that produced by the first and second bending modes was in the 0- to 40-cycle-per-second range, the difference of the data from unity is due primarily to motion in the sting and two rigid-body modes. The data in figure 9 indicate that the support system (including sting and flex springs) used for the model of this investigation was satisfactory in that no appreciable extraneous bending moments were produced.

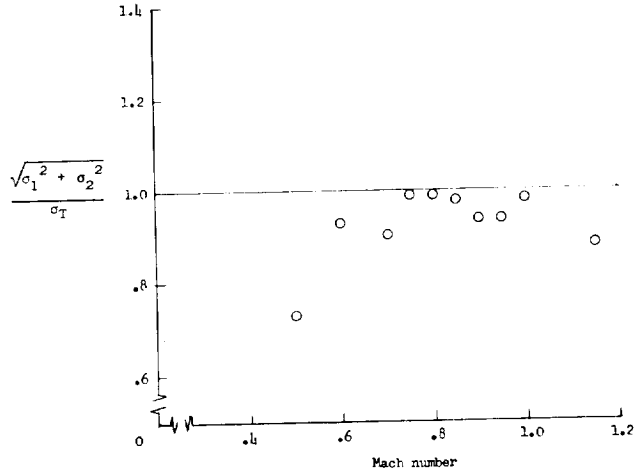

Figure 9.- Comparison of root-mean-square bending moment at strain-gage location attributable to first two free-free bending modes with total root-mean-square bending moment at strain-gage location for configuration 2.

For purposes of illustration the bending moments measured on configuration 2 at the strain-gage location have been extrapolated to full-scale values by using the scaling relationships presented in the "Analysis" section. The following assumptions have been made: first, a hypothetical full-scale vehicle has been selected such that the model-to-full-scale relationships are as shown in table IV; second, a typical orbital launch trajectory for such a vehicle has been assumed during which the vehicle weight, free-free bending frequencies, control-system damping, and aerodynamic damping vary with Mach number as indicated in table IV; finally, the full-scale structural damping was assumed to be the same as that measured for the model. The aerodynamic damping ratios for the first mode at Mach numbers from 0.90 to 1.2 were estimated from the aerodynamic damping measurements made on this configuration previously and reported in reference 7. Since no damping measurements were made for the first mode below $M = 0.90$, and none were made for the second mode at any Mach number, the aerodynamic damping below $M = 0.90$ in the first mode and throughout the Mach number range for the second mode was assumed to be the same as that measured for configuration 1. (See ref. 7.)

The predicted variation with Mach number of the full-scale root-mean-square bending moments at the strain-gage location for the first two bending modes is shown in figure 10. Also included in the figure is the variation of the total root-mean-square bending moment attributable to the first two bending modes. It may be seen from the figure that for a model test stagnation pressure of 600 pounds per square foot in the Mach number range from about 0.85 to 1.00 the second mode provides the major contribution to the total bending moment whereas outside this range the first mode predominates. Also shown in figure 10 are the predicted full-scale moments from the model test at $M = 0.90$ and $p_t = 1{,}800$ pounds per square foot. Although the amount of bending moment

TABLE IV.- ASSUMED FULL-SCALE CHARACTERISTICS

AND SCALING RELATIONSHIPS

Scaling relations assumed for M = 0.90:

$$\frac{L_M}{L_F} = 0.04 \qquad \frac{W_M}{W_F} = \left(\frac{L_M}{L_F}\right)^3\left(\frac{\rho_M}{\rho_F}\right) = 6.714 \times 10^{-5}$$

$$\frac{V_M}{V_F} = 1.00 \qquad \frac{f_M}{f_F} = \left(\frac{L_F}{L_M}\right)\left(\frac{V_M}{V_F}\right) = 25.0$$

$$\frac{\rho_M}{\rho_F} = 1.049 \qquad \frac{q_M}{q_F} = \left(\frac{\rho_M}{\rho_F}\right)\left(\frac{V_M}{V_F}\right)^2 = 1.049$$

M	q, lb/ft^2	W, lb	f_1, cps	f_2, cps	$\left(\frac{C_s}{C_{cr}}\right)_1$	$\left(\frac{C_s}{C_{cr}}\right)_2$	$\left(\frac{C_c}{C_{cr}}\right)_1$	$\left(\frac{C_c}{C_{cr}}\right)_2$	$\left(\frac{C_A}{C_{cr}}\right)_1$	$\left(\frac{C_A}{C_{cr}}\right)_2$
0.50	233	361,000	2.78	7.26	0.0110	0.0100	0.0100	0.0020	0.0022	0.0022
.60	310	347,000	2.89	7.54	.0110	.0100	.0104	.0024	.0022	.0022
.70	400	336,000	2.98	7.78	.0110	.0100	.0108	.0028	.0023	.0023
.75	450	331,000	3.03	7.90	.0110	.0100	.0110	.0030	.0024	.0024
.80	500	326,000	3.07	8.01	.0110	.0100	.0112	.0032	.0024	.0024
.85	540	322,000	3.11	8.11	.0110	.0100	.0114	.0034	.0025	.0025
.90	575	317,000	3.16	8.24	.0110	.0100	.0116	.0036	.0070	.0021
.95	608	313,000	3.20	8.35	.0110	.0100	.0118	.0038	-.0008	.0021
1.00	635	310,000	3.23	8.42	.0110	.0100	.0120	.0040	-.0002	.0019
1.15	698	299,000	3.35	8.74	.0110	.0100	.0126	.0046	.0005	.0018

contributed by each of the modes has changed slightly, the total bending moment is about the same as that determined from the model tests at the lower stagnation pressure. It is seen that the peak value of the bending moment occurs at about M = 0.95.

Of course, the designer is interested in more than the variation of the buffet bending moment at some particular vehicle station with Mach number. The distribution of the buffet bending moments along the vehicle must be known in order that the design bending-moment distribution (the buffet portion of which is usually based on a 3σ or other appropriate factor) may be determined. In figure 11 the longitudinal distribution of the total full-scale root-mean-square bending moments due to response in the first and second free-free bending modes are presented for Mach numbers of 0.70 and 0.95. These data were generated by using the results for the individual modes presented in figure 10 in conjunction with the bending-moment distributions given in figure 6. As is seen from figure 11, the two distributions are somewhat dissimilar. At the lower Mach number the major contribution to the total moment was made by the first mode. As a result, the shape of the moment distribution was very similar to the first-mode moment distribution presented in figure 6. At M = 0.95 the contribution of the second mode was substantial, and this condition resulted in the "saddleback" shape of the moment distribution. This figure illustrates the importance of higher bending modes in buffet bending-moment measurements on launch vehicles.

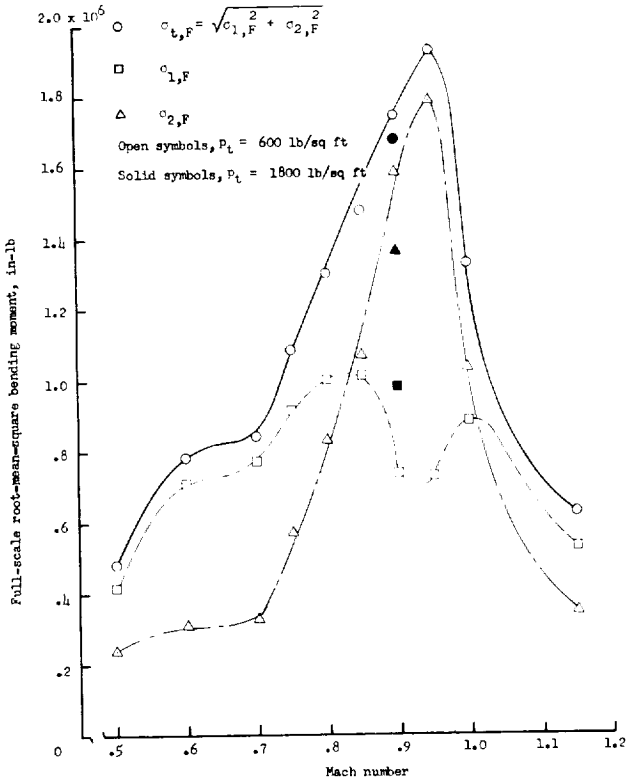

Figure 10.- Variation of full-scale root-mean-square bending moment at strain-gage location with Mach number obtained from tests on model configuration 2.

CONCLUDING REMARKS

A method for determining directly the overall dynamic response in terms of bending moment of an aeroelastic model of a launch vehicle to random (buffet) aerodynamic forces has been applied to two model configurations in the Mach number range from 0.50 to 1.20. The two configurations tested were a blunted cone-cylinder and a bulbous nose with a cylindrical afterbody. The cone-cylinder configuration was free from buffet over the range covered in this investigation. Significant buffet response was measured on the bulbous nose configuration. For

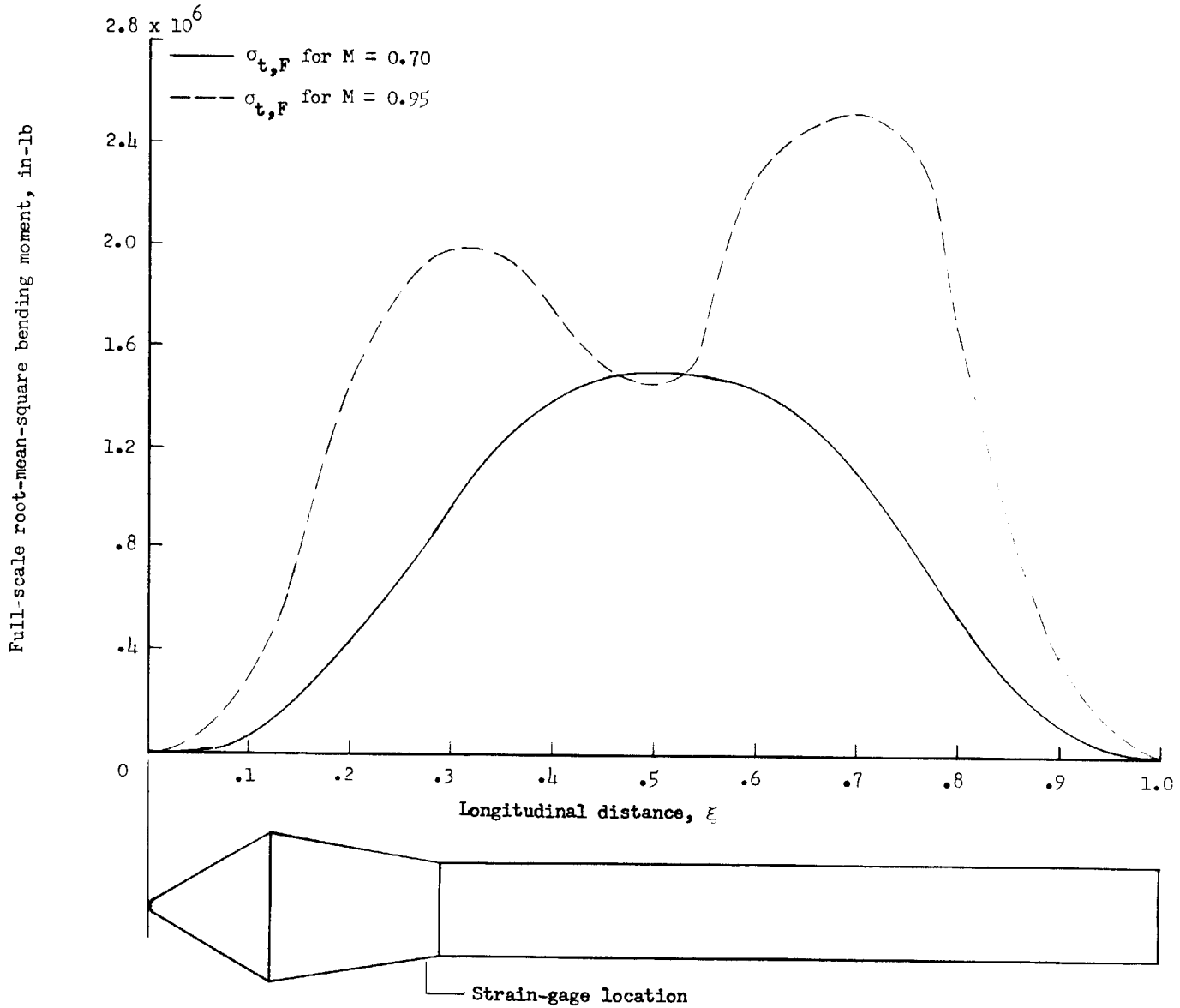

Figure 11.- Distribution of full-scale root-mean-square bending moment attributable to first two free-free bending modes at Mach numbers 0.70 and 0.95 obtained from model tests on configuration 2.

this configuration the total buffet response was composed of components associated with the first and second free-free bending modes.

Presented in the appendix is an analysis using the techniques of generalized harmonic analysis which develops in some detail the relationships necessary for predicting full-scale buffet bending moments from data obtained from wind-tunnel tests on dynamically scaled aeroelastic models.

It remains desirable, of course, to evaluate the aeroelastic model approach by direct comparison of model and full-scale results; however, suitable flight data for this purpose are not available.

Langley Research Center,
National Aeronautics and Space Administration,
Langley Station, Hampton, Va., August 8, 1963.

APPENDIX

DYNAMIC ANALYSIS OF BUFFETING WITH EMPHASIS ON SCALING MODEL DATA TO FULL-SCALE RESPONSE

The purpose of this appendix is to examine a launch vehicle which is subjected to a random (buffet) aerodynamic loading. The method of generalized harmonic analysis, which is treated in some length in reference 9 and was first applied to the analysis of buffeting in reference 10, provides the basis for this study. The vehicle is assumed to be flying at constant altitude with constant velocity. The only aerodynamic forces present in addition to the random component are damping forces proportional to the velocity of the bending vibrations of the system. No loss of generality results from neglecting the aerodynamic inertia and spring forces since such forces usually are small when compared with their structural counterparts for a slender launch vehicle.

The set of differential equations which govern the free-free bending vibration characteristics of the system under consideration is

$$M_n\ddot{a}_n(t) + C_n\dot{a}_n(t) + \omega_n^2 M_n a_n(t) = qRL \int_0^1 c_L(\xi,t)\, h_n(\xi)\, d\xi \qquad (n = 1, 2, 3, \ldots) \tag{1}$$

where

$a_n(t)$ nose deflection in nth bending mode

C_n generalized damping coefficient in nth bending mode, including aerodynamic, control system, and structural components

M_n generalized mass in nth bending mode

ω_n natural circular frequency in nth bending mode

The right-hand side of equation (1) is the generalized random aerodynamic load expressed in coefficient form. The function $c_L(\xi,t)$ is the random section lift coefficient and R, L, q, and $h_n(\xi)$ are, respectively, reference radius, vehicle length, free-stream dynamic pressure, and mode shape of nth bending mode referred to unity at the vehicle nose. The solution of equation (1) for the nose deflection is

$$a_n(t) = \frac{qRL \int_0^1 c_L(\xi,t)\, h_n(\xi)\, d\xi}{M_n\omega_n^2 \left\{\left[1 - \left(\frac{\omega}{\omega_n}\right)^2\right] + i\left[2\left(\frac{\omega}{\omega_n}\right)\left(\frac{C}{C_{cr}}\right)_n\right]\right\}} \tag{2}$$

or

$$a_n(t) = \frac{qRIA_n(\omega)\, \hat{c}_{L,n}(t)\, e^{-i\theta_n}}{M_n\omega_n^2} \tag{3}$$

where

$$A_n(\omega) = \frac{1}{\sqrt{\left[1 - \left(\frac{\omega}{\omega_n}\right)^2\right]^2 + \left[2\left(\frac{\omega}{\omega_n}\right)\left(\frac{C}{C_{cr}}\right)_n\right]^2}}$$

and is the square root of the mechanical admittance for the nth bending mode

$$\theta_n = \tan^{-1} \frac{2\left(\frac{\omega}{\omega_n}\right)\left(\frac{C}{C_{cr}}\right)_n}{1 - \left(\frac{\omega}{\omega_n}\right)^2}$$

and

$$\hat{c}_{L,n}(t) = \int_0^1 c_{L,n}(\xi,t)\, h_n(\xi)\, d\xi$$

The total deflection at the vehicle nose is

$$y(0,t) = qRL \sum_{n=1}^{\infty} \frac{A_n(\omega)\, \hat{c}_{L,n}(t)\, e^{-i\theta_n}}{M_n\omega_n^2} \tag{4}$$

The power spectrum of the nose amplitude is

$$\Phi_y(0,\omega) = \lim_{T\to\infty} \frac{1}{2\pi T} F\{y(0,t)\}\, F^*\{y(0,t)\} \tag{5}$$

where $F\{y(0,t)\}$ is the Fourier transform of the nose deflection and the asterisk indicates the complex conjugate of the Fourier transform. By employing equations (4) and (5), the spectrum of the nose displacement is

$$\Phi_y(0,\omega) = q^2R^2L^2 \sum_{n=1}^{\infty} \sum_{m=1}^{\infty} \frac{A_n(\omega)A_m(\omega)}{M_n\omega_n{}^2M_m\omega_m{}^2} C_{m,n}(\omega) \cos(\theta_n - \theta_m) \tag{6}$$

The function $C_{m,n}(\omega)$ is a correlation function and is defined by

$$C_{m,n}(\omega) = \lim_{T\to\infty} \frac{1}{2\pi T} F\left\{\hat{c}_{L,n}(t)\right\} F^*\left\{\hat{c}_{L,n}(t)\right\}$$

For a system with small damping and reasonably well separated natural frequencies, the cross terms ($m \neq n$) in equation (6) may be disregarded since all contributions to the total response are small except in the neighborhood of the resonant frequencies. Thus,

$$\Phi_y(0,\omega) = q^2R^2L^2 \sum_{n=1}^{\infty} \frac{A_n{}^2(\omega)}{M_n{}^2\omega_n{}^4} C_{L,n}(\omega) \tag{7}$$

where $C_{L,n}(\omega) = C_{n,n}(\omega)$. The mean-square nose deflection is

$$\overline{y(0,t)^2} = \int_0^{\infty} \Phi_y(0,\omega)\, d\omega \tag{8}$$

If $C_{L,n}(\omega)$ is reasonably constant in the vicinity of ω_n and the damping is small, a satisfactory approximation to the mean-square nose deflection may be made. This approximation is

$$\overline{y(0,t)^2} = q^2R^2L^2 \sum_{n=1}^{\infty} \frac{\pi\omega_n}{4M_n{}^2\omega_n{}^4\left(\frac{C}{C_{cr}}\right)_n} C_{L,n}(\omega_n) \tag{9}$$

In buffeting studies on elastic structures, usually the bending moment at some point on the structure, or the bending-moment distribution, is desired rather than the deflection of the structure. By using equation (9) and a set of coefficients which relate the bending moment in the nth bending mode to the nose amplitude in that mode, an expression for the mean-square bending moment may be

obtained. The bending moment at some longitudinal station ξ_o per unit nose deflection in the nth mode is

$$\omega_n^2 L^2 \int_0^{\xi_o} m(\xi)\left(\xi_o - \xi\right) h_n(\xi)\, d\xi$$

The expression for the total mean-square bending moment is

$$\sigma_T^2\left(\xi_o\right) = q^2 R^2 L^2 \sum_{n=1}^{\infty}\left[\frac{L^2 \int_0^{\xi_o} m(\xi)\left(\xi_o - \xi\right) h_n(\xi)\, d\xi}{M_n}\right]^2 \frac{\pi\omega_n}{4\left(\frac{C}{C_{cr}}\right)_n} C_{L,n}(\omega_n) \qquad (10)$$

The term enclosed in the brackets in equation (10) is an effective moment arm and is abbreviated as l_n. The contribution of the nth mode to the total moment is

$$\sigma_n^2\left(\xi_o\right) = l_n^2\left[\frac{\pi\omega_n}{4\left(\frac{C}{C_{cr}}\right)_n}\right] q^2 R^2 L^2 C_{L,n}(\omega_n) \qquad (11)$$

The right-hand side of equation (11) is the general term of the series in equation (10). The contribution of a single mode is essentially the same solution that would be obtained for a single-degree-of-freedom system subjected to a random loading. (See ref. 1.) Consequently, the total mean-square bending moment is a superposition of single-degree-of-freedom solutions, each mode being independently treated as a separate system. The right-hand side of equation (11) may be conveniently separated into three parts. The first term l_n^2, as previously mentioned, is the square of an effective moment arm. The second term, enclosed in brackets, is an admittance-type term. In particular, it is $\pi/2$ times the maximum value of the mechanical admittance in the nth mode multiplied by its width at the one-half power point. The damping ratio $\left(\frac{C}{C_{cr}}\right)_n$ which appears in this term is

$$\left(\frac{C}{C_{cr}}\right)_n = \left(\frac{C_A}{C_{cr}}\right)_n + \left(\frac{C_c}{C_{cr}}\right)_n + \left(\frac{C_s}{C_{cr}}\right)_n$$

where

$\frac{C_A}{C_{cr}}$ aerodynamic damping ratio

$\frac{C_c}{C_{cr}}$ control-system damping ratio

$\frac{C_s}{C_{cr}}$ structural damping ratio

In the notation of reference 7 the aerodynamic damping ratio is related to the effective aerodynamic damping derivative $C_{\dot{h}}$ by

$$\frac{C_A}{C_{cr}} = \frac{C_{\dot{h}}}{2\mu k} \tag{12}$$

The remaining terms in equation (11) are associated with the random aerodynamic loading. The function $C_{L,n}(\omega)$ is a correlation function. Or more precisely, it is the correlation function of the random section lift coefficients for the nth mode. Although not mathematically exact, a convenient way of thinking of this function is that it is the power spectrum of an effective random aerodynamic coefficient. The correlation function should be more properly expressed as a function of reduced frequency rather than as a function of frequency. From dimensional considerations,

$$C_{L,n}(\omega) = \frac{L}{V}\hat{C}_{L,n}(k_n) \tag{13}$$

where

$$k_n = \frac{L\omega_n}{V}$$

On substituting expressions (12) and (13) into equation (11) the mean-square bending moment in the nth mode becomes

$$\sigma_n^2(\xi_o) = l_n^2\left[\left(\frac{\pi\omega_n}{4}\right)\frac{1}{\left(\frac{C_s}{C_{cr}}\right)_n + \left(\frac{C_c}{C_{cr}}\right)_n + 2\pi R^2\left(\frac{C_{\dot{h}}}{C_{cr}}\right)_n\frac{q}{V}}\right]q^2R^2L^2\left(\frac{L}{V}\right)\hat{C}_{L,n}(k_n) \tag{14}$$

or upon combining and rearranging

$$\sigma_n^2(\xi_o) = \left(\frac{\pi}{4}L^2R^2l_n^2\right)k_n\left[\frac{1}{\left(\frac{C_s}{C_{cr}}\right)_n + \left(\frac{C_c}{C_{cr}}\right)_n + 2\pi R^2\left(\frac{C_{\dot{h}}}{C_{cr}}\right)_n\frac{q}{V}}\right]q^2\hat{C}_{L,n}(k_n) \tag{15}$$

The variation of the mean-square bending moment with dynamic pressure for a given Mach number is of interest. For the limiting case

$$\left(\frac{C_c}{C_{cr}}\right)_n = 0$$

$$\left(\frac{C_s}{C_{cr}}\right)_n = 0$$

$$\sigma_n^2(\xi_o) \propto q$$

and for vanishing aerodynamic damping

$$\left(\frac{C_c}{C_{cr}}\right)_n = 0$$

$$\left(\frac{C_{\dot{h}}}{C_{cr}}\right)_n = 0$$

$$\sigma_n^2(\xi_o) \propto q^2$$

In cases where both aerodynamic and structural damping must be considered, no simple proportionality relationship exists.

Equation (15) is useful in scaling bending-moment measurements on dynamically scaled aeroelastic models to full-scale values. Since k_n and $\hat{C}_{L,n}(k_n)$ would be the same for both the model and the full-scale vehicle, the full-scale moment for the nth mode is related to the corresponding model value by

$$\sigma^2(\xi_o)_{n,F} = \left(\frac{\Lambda_F}{\Lambda_M}\right)_n \frac{\left[\left(\frac{C_s}{C_{cr}}\right)_n + 2\pi R^2\left(\frac{C_{\dot{h}}}{C_{cr}}\right)_n \frac{q}{V}\right]_M}{\left[\left(\frac{C_s}{C_{cr}}\right)_n + \left(\frac{C_c}{C_{cr}}\right)_n + 2\pi R^2\left(\frac{C_{\dot{h}}}{C_{cr}}\right)_n \frac{q}{V}\right]_F} \frac{q_F^2}{q_M^2} \sigma^2(\xi_o)_{n,M} \qquad (16)$$

where the subscripts M and F refer to model and full-scale configurations, respectively, and

$$\frac{\Lambda_F}{\Lambda_M} = \frac{L_F^2 R_F^2 l_{n,F}^2}{L_M^2 R_M^2 l_{n,M}^2}$$

For a dynamically scaled aeroelastic model, the ratio Λ_F/Λ_F is merely the reciprocal of the geometric scale factor L_M/L_F raised to the sixth power.

The total full-scale mean-square bending moment in terms of model bending moment is

$$\sigma^2(\xi_o)_{T,F} = \sum_{n=1}^{\infty} \left(\frac{L_F}{L_M}\right)^6 \frac{\left[\left(\frac{C_s}{C_{cr}}\right)_n + 2\pi R^2 \left(\frac{C_h}{C_{cr}}\right)_n \frac{q}{V}\right]_M}{\left[\left(\frac{C_s}{C_{cr}}\right)_n + \left(\frac{C_c}{C_{cr}}\right)_n + 2\pi R^2 \left(\frac{C_h}{C_{cr}}\right)_n \frac{q}{V}\right]_F} \frac{q_F^2}{q_M^2} \sigma^2(\xi_o)_{n,M} \qquad (17)$$

It should be pointed out that expressions similar to equation (17) could be obtained for any quantity which is proportional to the displacement.

REFERENCES

1. Huston, Wilbur B., Rainey, A. Gerald, and Baker, Thomas F.: A Study of the Correlation Between Flight and Wind-Tunnel Buffeting Loads. NACA RM L55E16b, 1955.

2. Coe, Charles F.: Steady and Fluctuating Pressures at Transonic Speeds on Two Space-Vehicle Payload Shapes. NASA TM X-503, 1961.

3. Coe, Charles F.: The Effects of Some Variations in Launch-Vehicle Nose Shape on Steady and Fluctuating Pressures at Transonic Speeds. NASA TM X-646, 1962.

4. Jones, George W., Jr., and Foughner, Jerome T., Jr.: Investigation of Buffet Pressures on Models of Large Manned Launch Vehicle Configurations. NASA TN D-1633, 1963.

5. Goldberg, Arthur P., and Adams, Richard H.: Mercury-Atlas Buffeting Loads at Transonic and Low Supersonic Speeds. STL/TR-60-0000-AS431, Space Tech. Labs., Inc., Nov. 28, 1960.

6. Goldberg, A. P., and Wood, J. D.: Dynamic Loads in the Atlas-Able 5 During Transonic Buffeting. STL/TM-60-0000-19075, Space Tech. Labs., Inc., Aug. 22, 1960.

7. Hanson, Perry W., and Doggett, Robert V., Jr.: Wind-Tunnel Measurements of Aerodynamic Damping Derivatives of a Launch Vehicle Vibrating in Free-Free Bending Modes at Mach Numbers From 0.70 to 2.87 and Comparisons With Theory. NASA TN D-1391, 1962.

8. Hanson, Perry W., and Doggett, Robert V., Jr.: Aerodynamic Damping of a 0.02-Scale Saturn SA-1 Model Vibrating in the First Free-Free Bending Mode. NASA TN D-1956, 1963.

9. Rice, S. O.: Mathematical Analysis of Random Noise. Pts. I and II. Bell System Tech. Jour., vol. XXIII, no. 3, July 1944, pp. 282-332; Pts. III and IV, vol. XXIV, no. 1, Jan. 1945, pp. 46-156.

10. Liepmann, H. W.: On the Application of Statistical Concepts to the Buffeting Problem. Jour. Aero. Sci., vol. 19, no. 12, Dec. 1952, pp. 793-800, 822.